Progress In Electromagnetics Research M, Vol. 68, 153–161, 2018

UWB-SP Standard Transducer Based on Microstrip Line

Jin-Hong Wei*, You-Jie Yan, Shou-Long Zhang, Jin Chen, and Zhan-Jun Liu

Abstract—In this paper, an ultra-wideband standard transducer based on microstrip line is developed for the accurate measurement and metrology of UWB-SP. The transducer consists of a section of microstrip line and a section of coaxial line connected to the microstrip line via an SMA connector. The initial part of the transducer is chosen to receive the excitation signal, in order to expand the effective time window. Simulated results show that the waveform recovered by the transducer is almost coincident with the waveform of the excited electric field within the effective time window, and the upper frequency of the bandwidth is up to 3.5 GHz. Measured results show that the transducer can recover the waveform of the incident electric field very well. Additionally, the sensitivity and time window can be calibrated readily and accurately by the vector network analyzer as well as the UWB TEM cell. The experimental results are in good agreement with the theoretical and simulated ones.

1. INTRODUCTION

UWB-SP is a special electromagnetic pulse, which has faster rise time and shorter duration than High-altitude Electromagnetic Pulse (HEMP). For typical ultrashort electromagnetic pulse (UWB-SP) fields [1–5], the rise time is from several decuple ps to ns; the duration time is from several hundred ps to several ns; the spectrum of the field is up to 3 GHz or even more.

For metrology purpose, TEM horn is recommended by NIST as the receiving antenna [6]. It outputs a voltage waveform, which is identical to the incident electric field. However, the sensitivity of TEM horn is incalculable analytically and has to be calibrated by a standard field or a multi-antenna method. When used in a narrow space, TEM horn could be too large to ignore the disturbance to the external electric field caused by the receiving antenna.

Another receiving antenna that is also used for metrology is an asymptotic conical dipole (ACD) antenna [7]. ACD antenna is very small in size and has analytical sensitivity theoretically. However, near the center of the ACD antenna the structure should have a biconical shape, which is unlikely to be put into practice. Therefore, there is a biggish discrepancy between the calculated and practical sensitivities. In addition, due to the derivative behavior of this type of antenna, an integrator or a numerical integration has to be used to restore the pulse shape of the electric field, which either increases the complexity of the system or leads to the offset problem [8, 9].

A new UWB-SP standard transducer based on microstrip line is developed in this paper. The transducer consists of a section of microstrip line and a section of coaxial cable connected to an SMA connector, which has a good performance in aspects of bandwidth and dimension. The output signal of the transducer can replicate the waveform of the radiated pulsed electric field. There is no need to integrate the output signal. The designed structure of the transducer can be realized perfectly, and the sensitivity can be calibrated readily and accurately. The presented transducer shows advantages of small volume, fast rising time and good waveform fidelity [10, 11]. Details of the transducer design are described, and both simulated and measured results are presented in the following sections.

Received 17 March 2018, Accepted 28 April 2018, Scheduled 15 May 2018
* Corresponding author: Jin-Hong Wei (17600809313@163.com).
The authors are with the Northwest Institute of Nuclear Technology, Xi'an 710024, China.

2. TRANSDUCER DESIGN

The microstrip line considered is depicted in Fig. 1, where a microstrip line of length l and characteristic impedance Z_c illuminated by a time-harmonic uniform plane wave are shown. An ideal structure with a perfect conducting ground plane of width a, a metal conductor of width w, and a lossless dielectric substrate of thickness h and relative dielectric permittivity ε_r is assumed. The metal conductor is believed to be homogeneous along its length (the z coordinate). The conductor and ground plane are separated by the dielectric substrate and situated in free space. Both ends of the microstrip line are loaded with the loads Z_1 and Z_2 respectively, whose impedances are ohmic.

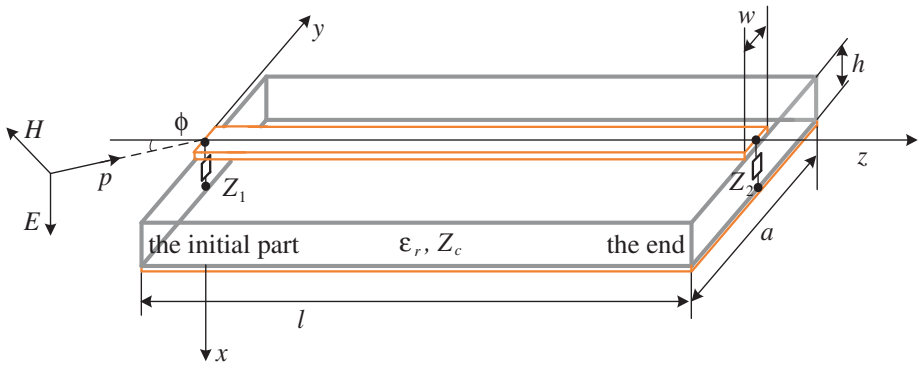

Figure 1. Microstrip line illuminated by a linearly polarized uniform plane wave.

The transmission line equations (telegrapher's equations) have been derived electrogynamically for the transmission line of two parallel homogeneous conductors separated by a dielectric layer and excited by an electromagnetic field [12–15]. We assume that $w \ll a$, $h \ll l$, $h \ll a$, then the microstrip line considered can be equivalent to the transmission line. Based on the transmission line equations, the excitation of the microstrip line by an external electromagnetic field is considered for Z_1 and Z_2. Under the condition that the vector E is perpendicular to the upper surface of the dielectric substrate, and the poynting's vector P is parallel to the surface, the equations are representable in the form

$$\begin{aligned} u(0,t) &= \frac{E_0 h(\rho_1+1)}{2}\sum_{k=0}^{\infty}(\rho_1\rho_2)^k \\ &\cdot\left\{\rho_2\left[\frac{\left(1-\frac{1}{\varepsilon_r}\right)\cos\phi}{\sqrt{\varepsilon_e}-\cos\phi}-\frac{1}{\varepsilon_r}\right]\cdot\left[f\left(t-\frac{(2k+1)l\sqrt{\varepsilon_e}+l\cos\phi}{c}\right)-f\left(t-\frac{2l(k+1)\sqrt{\varepsilon_e}}{c}\right)\right]\right. \\ &\left.-\left[\frac{\left(1-\frac{1}{\varepsilon_r}\right)\cos\phi}{\sqrt{\varepsilon_e}+\cos\phi}+\frac{1}{\varepsilon_r}\right]\cdot\left[f\left(t-\frac{2kl}{c}\right)-f\left(t-\frac{(2k+1)l\sqrt{\varepsilon_e}+l\cos\phi}{c}\right)\right]\right\} \end{aligned} \quad (1)$$

$$\begin{aligned} u(l,t) &= \frac{E_0 h(1+\rho_2)}{2}\sum_{k=0}^{\infty}(\rho_1\rho_2)^k \\ &\cdot\left\{\left[\frac{\left(1-\frac{1}{\varepsilon_r}\right)\cos\phi}{\sqrt{\varepsilon_e}-\cos\phi}-\frac{1}{\varepsilon_r}\right]\cdot\left[f\left(t-\frac{2lk\sqrt{\varepsilon_e}+l\cos\phi}{c}\right)-f\left(t-\frac{(2k+1)l\sqrt{\varepsilon_e}}{c}\right)\right]\right. \\ &\left.-\rho_1\left[\frac{\left(1-\frac{1}{\varepsilon_r}\right)\cos\phi}{\sqrt{\varepsilon_e}+\cos\phi}+\frac{1}{\varepsilon_r}\right]\cdot\left[f\left(t-\frac{(2k+1)l\sqrt{\varepsilon_e}}{c}\right)-f\left(t-\frac{2l(k+1)\sqrt{\varepsilon_e}+l\cos\phi}{c}\right)\right]\right\} \end{aligned} \quad (2)$$

where $u(0,t)$ and $u(l,t)$ are the voltages of loads Z_1 and Z_2, respectively. E_0 is an external field strength of the incidence wave outside the dielectric substrate, f a function determining the pulse waveform, ε_r a

relative dielectric permittivity of the substrate, ε_e an equivalent dielectric permittivity of the microstrip line, and c a velocity of wave propagation in the environment. ρ_1 and ρ_2 are respectively the reflection coefficients at the initial part and the end of the microstrip line

$$\rho_1 = \frac{Z_1 - Z_c}{Z_c + Z_1}, \quad \rho_2 = \frac{Z_2 - Z_c}{Z_c + Z_2} \tag{3}$$

From Eq. (1), the load voltage $u(0,t)$ is the sum infinite series, in which the attenuation coefficient is $\rho_1\rho_2$, and the period is $2l\sqrt{\varepsilon_e}/c$. It corresponds to the superposition of a series of voltage signals with different amplitudes and different delay times. The incidence wave front reaches the impedance Z_1 at a time $t_0 = 0$. Under the action of the external field, the first voltage signal arises on the load Z_1, and the waveform of the voltage signal is consistent with the waveform of the external field. After time $t_0 = 0$, the external field will propagate in the environment with the velocity c from the initial part of the microstrip line to the end, then the incidence wave front reaches the impedance Z_2 at a time $t_1 = l\cos\phi/c$. Under the action of the external field, the second voltage signal arises on the load Z_2. The corresponding current signal arising on Z_2 will transmit along the microstrip line from Z_2 to Z_1 with the velocity $c/\sqrt{\varepsilon_e}$. After a time $t_2 = l\sqrt{\varepsilon_e}/c$, the current signal arrives at the impedance Z_1, and the corresponding voltage signal adds together with the first voltage signal. Thus the first voltage signal will remain on the impedance Z_1 during a time

$$t_{w1} = \frac{l\sqrt{\varepsilon_e} + l\cos\phi}{c} \tag{4}$$

Similarly, from formula (2), the first signal from the load voltage $u(l,t)$ will remain on the impedance Z_2 during a time

$$t_{w2} = \frac{l\sqrt{\varepsilon_e} - l\cos\phi}{c} \tag{5}$$

t_{w1} and t_{w2} are respectively the effective time windows of both ends. The incident signal can be recovered by the microstrip line when the time window is long enough. Since $t_{w1} > t_{w2}$, we choose the initial part of the microstrip line to record the first voltage signal (the incident electric field). If the bottom width of the measured pulse is $\Delta\tau$, length l of the microstrip line can be determined by

$$l > \frac{c\Delta\tau}{\sqrt{\varepsilon_e} + \cos\phi} \tag{6}$$

Therefore, bigger ε_e means shorter length l of the microstrip line. After determining the dielectric substrate, the transducers with different time windows can be designed by changing the length of the transducer to meet the measurement requirements of UWB-SP of different pulse durations. Within the effective time window, the relation between the recovered voltage signal $U(t)$ of the transducer and the excited electric field $E(t)$ can be simply expressed as

$$U(t) = h_{ef}E(t) = \frac{h(\rho_1+1)}{2}\left[\frac{\left(1-\frac{1}{\varepsilon_r}\right)\cos\phi}{\sqrt{\varepsilon_e}+\cos\phi} + \frac{1}{\varepsilon_r}\right]E(t) \tag{7}$$

In formula (7), h_{ef} is the sensitivity of the transducer, which is mainly determined by thickness h and reflection coefficient ρ_1. In addition, converting formula (7) to the frequency domain, we can see that the bandwidth of the transducer is related to the reflection coefficient $\rho_1(w)$.

Figure 2 shows the geometry of the proposed standard transducer. The transducer is based on microstrip line with the characteristic impedance $50\,\Omega$. The conductor is printed on a microwave composite substrate of relative permittivity 9.8 and loss tangent less than 0.001. The ground plane is printed on the other side of the substrate. On the initial part of the microstrip line, a $50\,\Omega$ SMA connector is connected to the metal conductor and grounded to the bottom of the ground plane, and then the SMA connector connects with a semi flexible cable for signal transmission. On the other end of the microstrip line, the conductor and ground plane are separated by the substrate. In this design, a thick substrate is chosen to produce a higher sensitivity h_{ef}. By shortening the distance Lf between the feeding position and the beginning of microstrip line, a longer time window and a wider bandwidth are achieved. Moreover, the change in thickness of the conductor will lead to a change of sensitivity

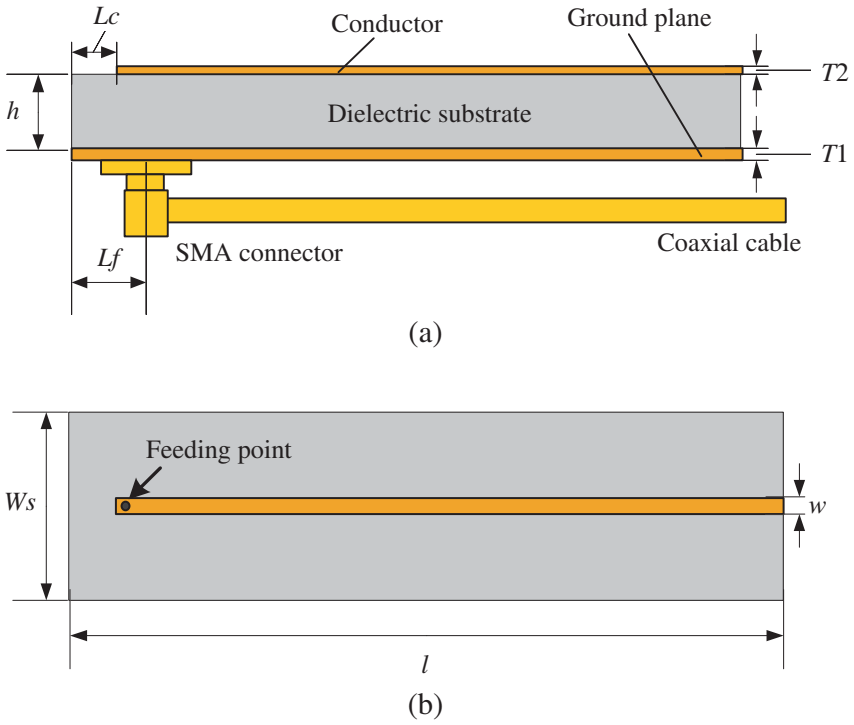

Figure 2. Geometry of proposed transducer, (a) side view and (b) top view.

h_{ef}. So the thin metal conductor is adopted to decrease the effect on the sensitivity h_{ef}. As illustrated in Fig. 2, in order to avoid the coupling effect from the external electromagnetic environment, the cable is placed in parallel with the ground plane of the transducer.

In consideration of the bandwidth, the sensitivity and the realizability of the transducer, an appropriate microstrip transducer is designed with parameters shown in Table 1.

Table 1. Optimal parameter values of the transducer.

Parameter	symbol	Value/mm
Microstrip line length	l	310
Substrate thickness	h	3.175
Substrate width	ws	50
Ground plane thickness	$T1$	0.035
Conductor thickness	$T2$	0.035
Conductor width	w	3
Feeding position	Lf	10
Conductor position	Lc	8

3. PERFORMANCE SIMULATION

In this section, the performances of the proposed transducer are analyzed by the Microwave CST studio, which is based on the finite integration technique (FIT) [16]. Linear polarization plane wave is set as the excitation source in the simulation. The direction of the electric field is perpendicular to the upper surface of the ground plane. Instead of the oscilloscope, a matched load is connected to the end of the

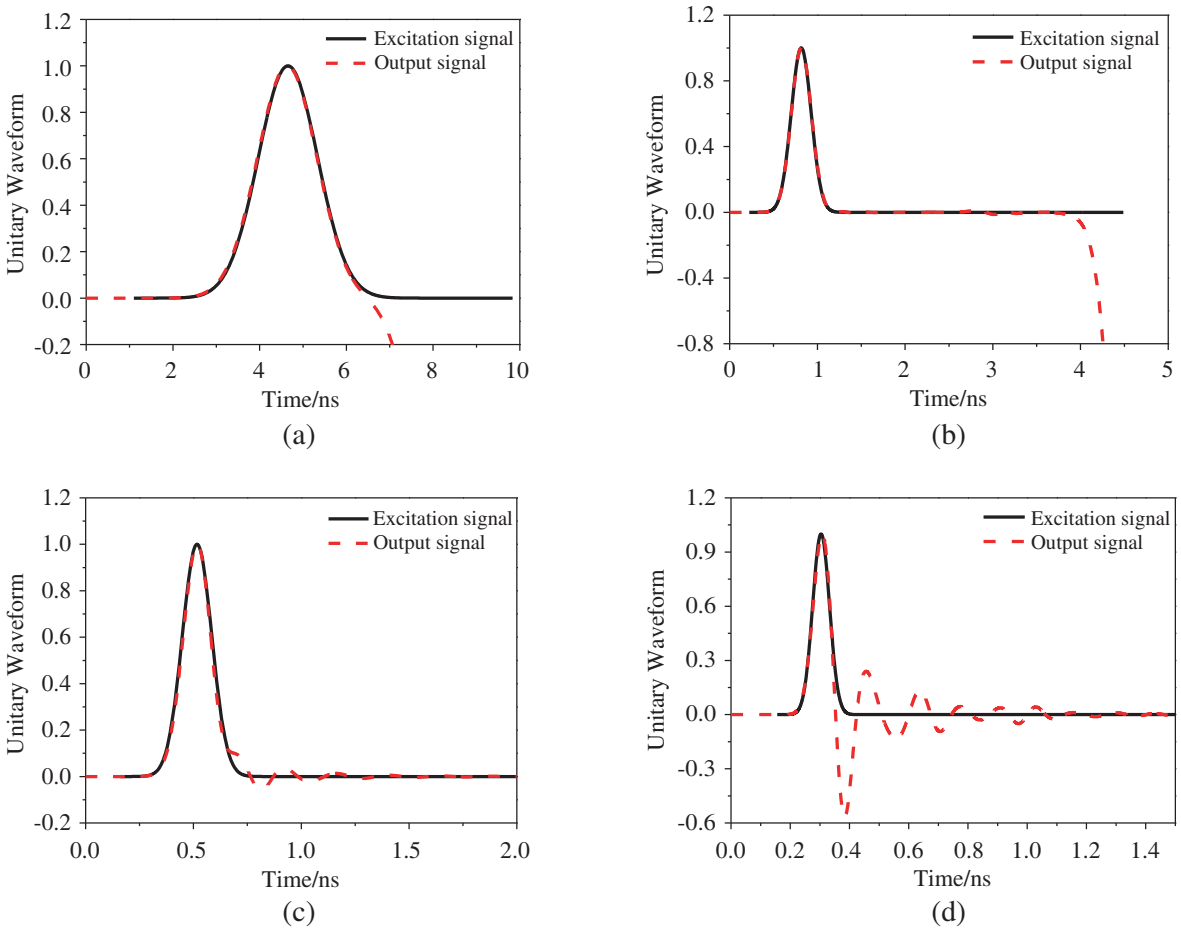

Figure 3. Excitation signals and output signals under the excitation of Gaussian pulses with different pulsewidth, (a) 2.9 ns, (b) 0.5 ns, (c) 0.3 ns and (d) 0.12 ns.

coaxial line to get the output signal.

In Fig. 3, the output waveforms obtained from the transducer are calculated under the excitation of Gaussian pulses with different pulsewidth. It can be seen from Figs. 3(a)–3(c) that the effective time window is 3.6 ns. For a series of incident Gaussian pulses with bottom width of 0.3 to 2.9 ns, the transducer has enough time window to recover the excitation pulses, and the recovered waveform almost completely coincides with the incident electric field waveform. Between the recovered waveform and incident waveform, the discrepancy of pulse width is less than 1%; the discrepancy of the rise time and the discrepancy of the drop time are less than 2%. For the waveforms beyond the effective time window shown in Figs. 3(a) and 3(b), it is from the voltage signal arising on the end. The signal transmits along the microstrip line from the end to the initial part, then adds together with the recovered signal.

Under the excitation of a monopole Gaussian pulse with a bottom width of 0.12 ns and a rise time of 50 ps, the recovered waveform and incident waveform are compared in Fig. 3(d). As shown in Fig. 3(d), the discrepancy of pulse width is 1.7%. The discrepancy of rising time is 0.9%, which reveals that the rise time of the transducer is about 50 ps.

Under the excitation of a monopole pulse with an upper frequency 4.3 GHz, we convert the recovered signal and excitation signal to the frequency domain, then the transfer function of the transducer can be calculated. It can be seen from Fig. 4 that when frequencies is less than 3.5 GHz, the amplitude response is almost flat, and the phase response is linear, which signifies that the transducer has a wide bandwidth from DC to 3.5 GHz. In this frequency range, the transducer has a high fidelity. The simulated sensitivity of the transducer is about 0.56 mm, which is consistent with the theoretical result of $\rho_1 = 0$. It should be noticed that the transducer needs to change the length to satisfy the measurement for the UWB-SP with the upper frequency less than 3.5 GHz and the bottom width larger than 3.6 ns.

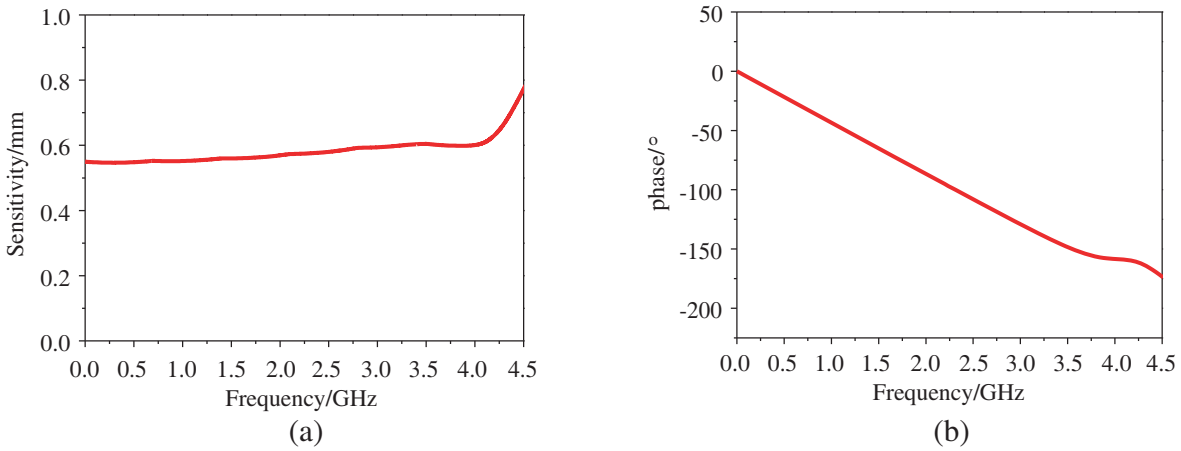

Figure 4. Transfer function of the transducer, (a) amplitude response, (b) phase response.

4. EXPERIMENT RESULT AND DISCUSSION

Based on the selected parameters, the UWS-SP transducer has been constructed. A photograph of the transducer is exhibited in Fig. 5.

Figure 5. The photograph of transducer.

The transducer is measured in a UWB TEM cell [17, 18]. The experiment system is built up as shown in Fig. 6. It is composed of an impulse source, a UWB TEM cell, a power divider, an attenuator, optical fiber, and oscilloscope, etc. The TEM cell is produced by a mono-conical antenna which consists of an aluminous cone with half cone-apex angle $\theta_c = 47°$ (the corresponding characteristic impedance $Z_c = 50\,\Omega$) and generatrix length of 1.5 m, and an aluminous ground plane with the size 3 m × 3 m. The TEM cell can form a standard UWB-SP field and have an equivalent time window of 5 ns, which means that during a time of 5 ns the waveform of the electric field in the TEM cell is identical to the feeding voltage waveform.

The pulse produced by the impulse source is sent by cable 1 to an ANRITSU K241B POWER SPLITTER. The reference signal u_s from one port of the splitter is sent into an attenuator and then recorded by channel 1 of the LeCroy WaveMaster 8620A oscillograph with a bandwidth of 6 GHz and sample speed of 20 GS/s. The voltage signal from another port excites the TEM cell through cable 2 and the feed structure to form an EM field between the cone and ground plane. We put the transducer into the operating zone of the monocone at a distance $r = 0.4$ m from the feeding point and an angle $\theta = 80°$ from the central axis of the cone, and keep the direction of the electric field perpendicular to the upper surface of the transducer and the initial part of the transducer aimed to the feeding point of the TEM cell. The output signal u_r of the transducer is sent into the channel 2 of the oscillograph.

The single peak pulse with a pulse width of 250 ps and an upper frequency of 3.8 GHz, and the double peak pulse with a peak-to-peak width of 1 ns and an upper frequency of 1.8 GH are adopted respectively as excitation signals. The output waveforms of the transducer and reference waveforms are

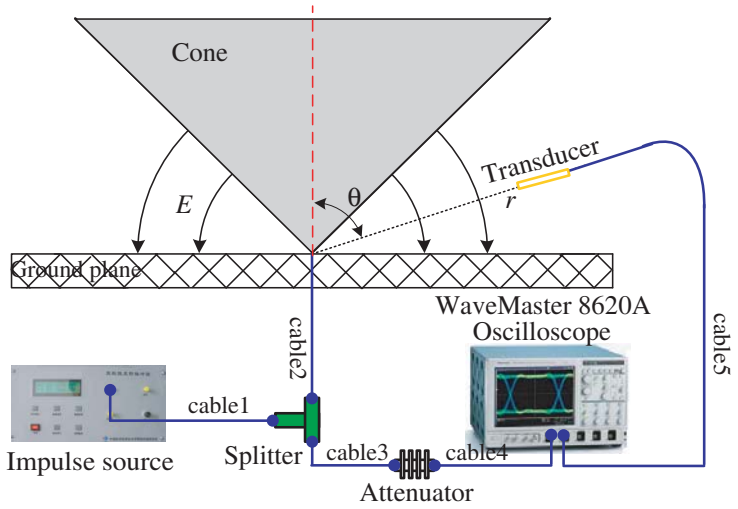

Figure 6. Experiment system.

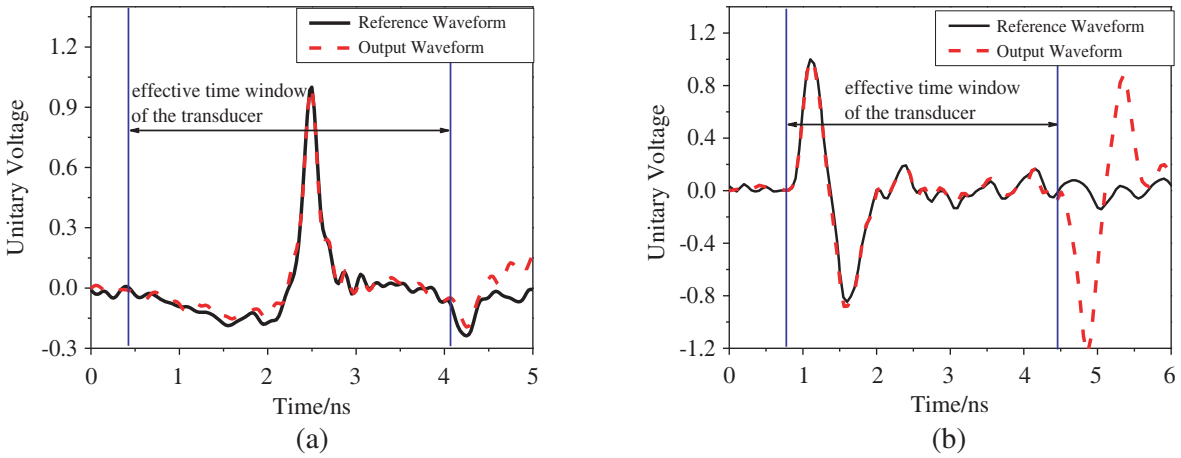

Figure 7. Result of the transducer fidelity. (a) Single peak pulse as excitation, (b) double peak pulse as excitation.

compared in Fig. 7. As shown in Fig. 7, the effective time window of the transducer is 3.6 ns, which is in agreement with the simulated result as well as the theoretical result. Moreover, within the effective time window, the recovered waveforms coincide with the reference waveforms very well.

The electric field $e(t)$ radiated by the TEM cell at the position located on the distance r and the angle θ can be expressed [17] as

$$e(t) = \frac{u_s}{r \sin\theta \ln\left(\cot\frac{\theta_c}{2}\right)} \tag{8}$$

Thus, the sensitivity of the transducer can be calibrated by the equation

$$h_{ef} = \frac{u_r r \sin\theta \ln\left(\cot\frac{\theta_c}{2}\right)}{u_s} \tag{9}$$

Before the calibration, not only the attenuation of coaxial cables and attenuator but also the imbalance of the splitter is measured in time domain, and then the measurement results are used to emend the calibration. After multiple calibrations, the sensitivity of the transducer is calculated from formula (9). As shown in Fig. 8, the measured result is 0.48 mm. The difference between the measured and theoretical or simulated results (0.56 mm) is 14%. The cause of the deviation is from the welding,

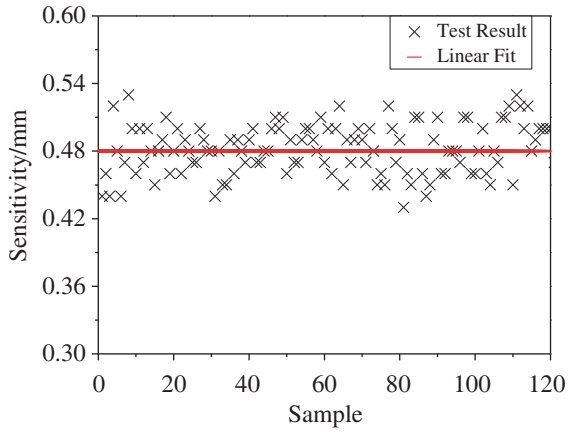

Figure 8. Sensitivity.

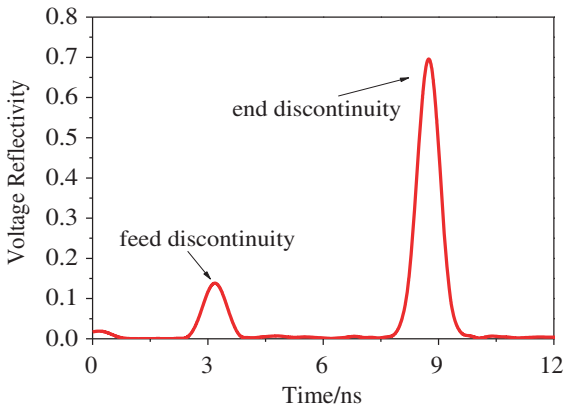

Figure 9. Impulses response of the feeding position.

positioning and other fabricating problems, which cause the reflection coefficient $\rho_1(w) \neq 0$ in a wide frequency band.

Therefore, an Agilent E8363B network analyzer is used to measure the impulse response of the feeding position of the transducer. The vector network analyzer has a built-in module for time domain analysis, which adopts the inverse chirp-z transform to transform the measured data in the frequency domain to the time domain [19]. Thus, the time domain response of the feeding position is obtained and shown in Fig. 9. According to the time and relative position of each reflection, we can see that the first reflection (the feed discontinuity) occurs on the feeding position of the transducer, and the second reflection (the end discontinuity) occurs on the end of the transducer. As shown in Fig. 9, the voltage reflection coefficient at the feeding position is 14%, then we can get $\rho_1 = -0.14$. Inserting ρ_1 into formula (7), we can obtain the sensitivity of the transducer. The result is also 0.48 mm, which is coincident with the measured result obtained in the UWB TEM cell. It reveals that the vector network analyzer as well as the UWB TEM cell can be used to calibrate the transducer accurately.

5. CONCLUSION

A UWB-SP transducer based on the microstrip line is designed, simulated and measured in this paper. In this design, the transducer consists of a microstrip line, an SMA connector and a coaxial cable. In order to expand the effective time window, the initial part of the microstrip line is chosen to connect the SMA connector for signal transmission. The effective time window of the presented transducer is 3.6 ns. The transducer can measure a series of UWB-SP with bottom width in the range of $0.3 \sim 2.9$ ns. In the frequency range from DC to 3.5 GHz, the sensitivity of the transducer is about 0.56 mm, and the transducer has a good fidelity for the excitation pulses of the spectrum in this range. The proposed transducer has a simple configuration and is easy to fabricate. The experimental results are in good agreement with the simulated and theoretical results. This validates that the transducer can be used as a standard transducer for the measurement and metrology of UWB-SP.

REFERENCES

1. Prather, W. D., F. J. Agee, and C. E. Baum, "Ultra-wideband sources and antennas," *Ultra-Wideband, Short-Pulse Electromagnetics*, Vol. 4, 119–130, Springer, US, 2002.
2. Prather, W. D., C. E. Baum, and J. M. Lehr, "Ultra-wideband source and antenna research," *IEEE Transactions on Plasma Science*, Vol. 28, No. 5, 1624–1630, October 2000.
3. Fedorov, V. M., E. F. Lebedev, V. Ye. Ostashev, V. P. Tarakanov, and A. V. Ul'yanov, "High power radiators for ultra-wideband electromagnetic impulses," *Progress In Electromagnetics Research Symposium*, 1476–1482, Moscow, Russia, August 19–23, 2012.

4. Baum, C. E., "From the electromagnetic pulse to high-power electromagnetics," *IEEE Trans. Electromagnetic Compatibility*, Vol. 80, No. 6, 789–817, 1992.
5. Barrett, W., "History of ultra wideband (UWB) radar & communication: Pioneers and innovators," *Progress In Electromagnetics Symposium*, 1–42, Cambridge, MA, July 2000.
6. Andrews, J. R., "UWB signal sources, antennas and propagation," *IEEE Topical Conference on Wireless Communication Technology*, 439–440, 2003.
7. Olsen, S. L., "Asymptotic conical dipole D-dot transducer (ACD-S1(R)) development," *EG&G Report*, No. AFWL-TR-75-263, April 1976.
8. Shen, H. M. and R. W. King, "New sensors for measuring very short electromagnetic pulses," *IEEE Transactions on Antennas and Propagation*, Vol. 38, No. 6, 838–846, 1990.
9. Yao, L. J., et al., "Compensation of the offset in numerical integration of a D-dot sensor measurement," *Proc. 3rd Asia-Pac. Conf. Antennas Propag.*, 898–901, Harbin, China, 2014.
10. Chen, J., "Ultra-wideband standard antenna for transient field measurement of short electromagnetic pulse," *Proc. of the 2013 International Symposium on Electromagnetic Compatibility*, 197–202, 2013.
11. Allen, O. E., D. A. Hill, and R. Arthur, "Time-domain antenna characterizations," *IEEE Trans. Electromagnetic Compatibility*, Vol. 35. No. 3, 339–34, 1993.
12. Podosenov, S. A., "Linear two-wire transmission line coupling to an external electromagnetic field. Part II: Specific cases, experiment," *IEEE Trans. Electromagnetic Compatibility*, Vol. 37, No. 4, 566–574, 1995.
13. Podosenov, S. A., "Linear two-wire transmission line coupling to an external electromagnetic field. Part I: Theory," *IEEE Trans. Electromagnetic Compatibility*, Vol. 37, No. 4, 559–566, 1995.
14. Ari, N. and W. Blumer, "Analytic formulation of the response of a two-wire transmission line excited by a plane wave," *IEEE Trans. Electromagnetic Compatibility*, Vol. 30, No. 4, 437–448, 1988.
15. Podosenov, S. A. and K. Yu. Sakharov, "Approximate calculation methods for pulse radiation of a TEM-horn array," *IEEE Trans. Electromagnetic Compatibility*, Vol. 43, No. 1, 67–74, 2001.
16. Microwave Studio (MWS) is a registered trademark of CST GmbH, Darmstadt, Germany.
17. Yan, Y. J. and X. L. Liu, "*E*-field generation setup for UWB-SP transducer calibration," *2012 Asia-Pacific Symposium on IEEE Electromagnetic Compatibility (APEMC)*, 541–544, 2012.
18. IEEE Standard for Calibration of Electromagnetic Field Transducers and Probes, Excluding Antennas, from 9 kHz to 40 GHz, IEEE Std. 1309$^{\text{TM}}$, 2005.
19. Bracewell, R. N. and R. N. Bracewell, *The Fourier Transform and Its Applications*, McGraw-Hill, New York, 1986.